

Mapping Cortical Connectivity Profiles Across the Human Brain

by

Gabriel Haw

VU ID: 2828156

Supervisor: Prof. Martijn van den Heuvel

Examiner: Dr. Solon Pissis



UNIVERSITY OF AMSTERDAM



*A thesis submitted in fulfillment of the requirements for
the joint UvA-VU Master of Science degree in Bioinformatics and Systems Biology,
Major Research Project Bioinformatics (XM_0103), 60EC*

June 2025

Abstract

The human cortex is organised along large-scale connectivity gradients, extending from primary unimodal regions (e.g., sensorimotor cortices) to transmodal areas involved in higher-order cognition. These gradients are thought to reflect basic organisational principles shaped by brain development, where spatial layout (Buckner and Krienen, 2013) and wiring cost (Sepulcre et al., 2010; Bullmore and Sporns, 2012) influence cortical specialisation. To explore these principles, we use variogram-based methods to measure spatial patterns of connectivity, capturing both the strength of local connections and the typical connection distances between regions. Our estimated connectivity profiles generally reflect a region's position along the established unimodal-transmodal gradient, with primary sensory regions showing strong, short-range connectivity and transmodal regions exhibiting weaker local connectivity and longer-range connections. Consistent with prior findings, we also identified regions with both high local connectivity and long-range projections, particularly in the posterior cingulate and medial prefrontal cortex, areas thought to function as core hubs of the default mode network (DMN) (Sepulcre et al., 2010; Leech and Sharp, 2014; Gowik et al., 2023). Furthermore, supporting the tethering hypothesis (Buckner and Krienen, 2013), we found that regions with longer-range connections tend to lie farther from primary sensory cortices. This supports the idea that connectivity and spatial constraints jointly shape cortical organisation, linking large-scale gradients to underlying developmental and evolutionary principles.

Introduction

Humans exhibit markedly larger brains relative to other mammals, with cerebral volumes approximately seven times greater than predicted for a mammal of comparable body mass, and nearly three times larger than those of other primates (Suntsova and Buzdin, 2020). Yet, this increase has not been uniform across all cortical regions. The cerebral cortex exhibits the most pronounced growth relative to other brain structures, particularly within regions identified as association cortices (Buckner and Krienen, 2013; Chin et al., 2023). These regions are crucial for integrating multi-sensory information and supporting higher cognitive functions such as abstract thinking,

decision-making, and complex social interactions (Preuss, 2011).

In contrast, evolutionary conserved primary sensory-motor cortices, involved in visual, auditory, and motor (see **Figure 1**) processing have been shown to occupy a progressively smaller proportion of the total cortical surface (Buckner and Krienen, 2013). This disproportionate growth in human association cortices highlights evolutionary pressures favoring this enhanced cognitive flexibility (Chin et al., 2023). The exact mechanisms underlying the expansion and preferential selection of specific cortical areas remain unclear.

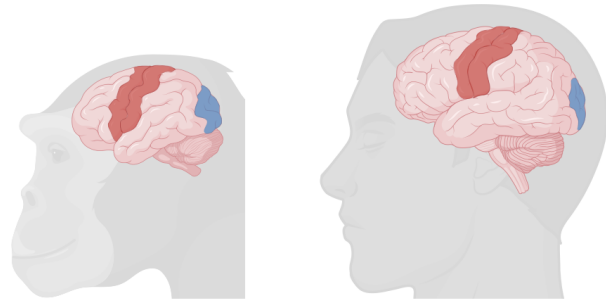


Figure 1: Primary somatomotor (red) and visual (blue) areas are highlighted on both chimpanzee (*Pan troglodytes*) and human (*Homo sapiens*) brains. The relative positioning and size of these regions appear highly conserved across species. Humans also exhibit a greater expansion of transmodal cortical territory between these primary sensory areas. Figure created with BioRender.

One potential explanation, initially proposed by Mesulam and further elaborated on by Buckner and Krienen (Mesulam, 1990; Buckner and Krienen, 2013), suggests that the evolution of association networks arose as a natural side effect of global brain expansion. The "tethering hypothesis" (Buckner and Krienen, 2013) posits that cortical organisation during early development is shaped by both molecular signals and incoming sensory inputs, resulting in the early maturation of primary sensory regions. These regions then act as developmental anchors, limiting how nearby parts of the brain grow and connect to other regions (Buckner and Krienen, 2013; Rosa and Tweedale, 2005). As the cortex expanded during mammalian evolution, regions located further from fixed sensory anchors may have become less constrained by early developmental gradients, facilitating the emergence of flexible, long-range association cortices (Buckner and Krienen, 2013). In line with this idea, regions of the default mode network (DMN), a

specialised set of areas supporting abstract cognition and higher-order cognitive functions, are situated at maximal distances from primary sensory cortices (Oligschläger et al., 2017, 2019). Although cortical connectivity predominantly favors short-range local connections due to lower wiring costs, regions involved in more cognitively demanding processes, including those in the default mode network (DMN), maintain extensive long-range connectivity despite the associated energy constraints (Oligschläger et al., 2017, 2019; Markov et al., 2011). A possible explanation is that the increased wiring cost of these long-range connections is offset by gains in network efficiency and integrative processing (Bullmore and Sporns, 2012; Collin et al., 2014; Hahn et al., 2015), potentially enabled by their increased distance from primary sensory areas (Oligschläger et al., 2017, 2019; Buckner and Krienen, 2013).

In this study, we assess whether there is a shift from strong, short-range connectivity in sensory areas to more distributed, long-range connectivity within transmodal regions of the cortex (Sepulcre et al., 2010; Oligschläger et al., 2017, 2019). Building on prior fMRI-based work (Oligschläger et al., 2017, 2019; Leech et al., 2023; Wang

et al., 2023), a variogram-based framework is applied to structural connectivity to assess whether spatial distance from primary anchors predicts changes in regional connectivity structure, as proposed by the tethering hypothesis (Buckner and Krienen, 2013). Variograms are a method for quantifying spatial structure by fitting a function to describe how values change with distance. In this context, they are used to characterise each region's connectivity profile as a function of distance, capturing how connection strength typically declines from nearby to more distant regions (Markov et al., 2011; Shinn et al., 2022; Leech et al., 2023). Two parameters are extracted from each profile: the sill, defined as the region's strongest connection and serving as a proxy for local connectivity strength, and the range, indicating the typical length of its connections. These parameters capture complementary aspects of a region's connectivity profile, how strongly it connects locally and how far its connections extend across the cortex. Drawing on prior work, we hypothesise that sensory regions exhibit stronger, more localised connectivity (higher sill, shorter range), whereas association regions show weaker but more spatially distributed connections (lower sill, longer range) (Sepulcre et al., 2010; Oligschläger et al., 2017, 2019).

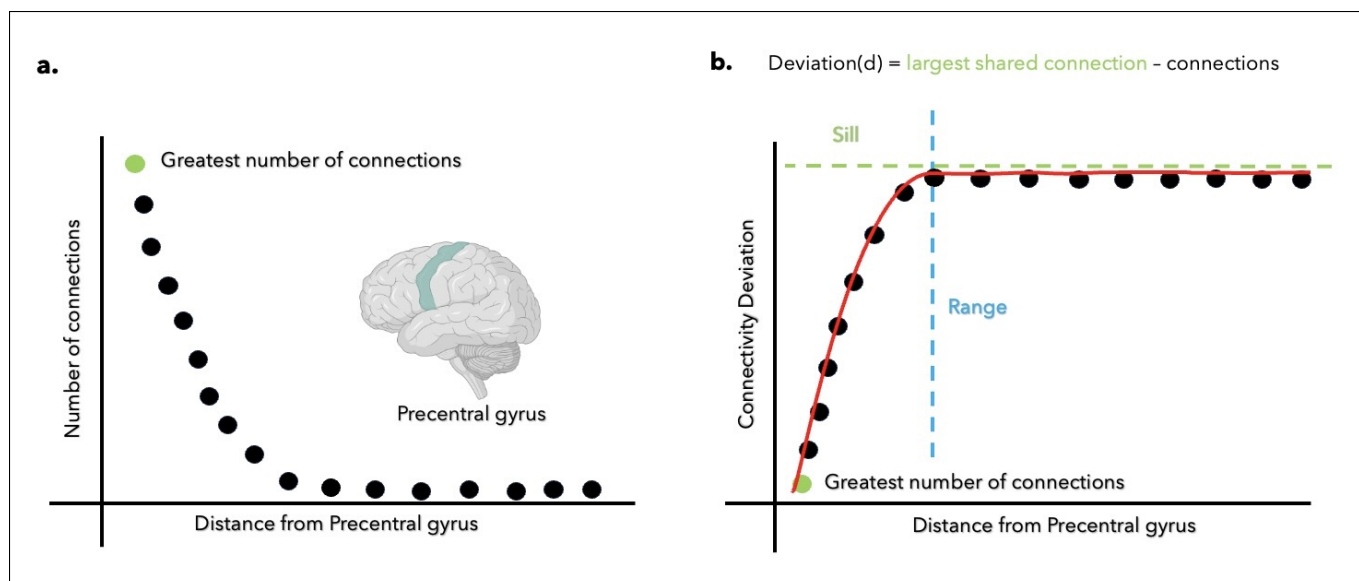


Figure 2: Illustration of spatial connectivity trend and deviation-based modeling. This figure shows an example of the spatial connectivity trend, using the precentral gyrus (colored region) as a reference region. Each black dot represents its shared connection to another region, positioned according to its geodesic distance from the precentral gyrus. The green dot marks the region with which it shares the greatest number of connections, typically observed at short distances (i.e., an adjacent region). **a.** Standard relationship between connectivity strength and distance, where the number of connections from the precentral gyrus to other regions decreases with increasing geodesic distance. **b.** To capture this trend quantitatively, connection strengths are transformed into a deviation profile, and a monotonic function (red line) is fitted to the data. This approach reflects the variogram-based analysis used in the study, which assumes that deviation increases with distance. By measuring how connection strength deviates relative to a region's strongest connection, two key parameters can be extracted. The **sill** (green line) is the maximum observed deviation, defined as the difference between a region's strongest connection and its weakest, where the weakest connection typically approaches zero at sufficient distance. As a result, the sill effectively reflects the region's strongest connection, thereby serving as a proxy for local connectivity strength. The **range** (light blue line) indicates the geodesic distance at which this deviation stabilises, reflecting the typical lengths of a region's connections. *Figure created with BioRender.*

Materials & methods

Imaging data and processing

An overview of the full methodological pipeline, including data processing and analysis steps, is provided in **Figure 3**. Functional and anatomical MRI data were obtained from the Center for Biomedical Research Excellence (COBRE). Imaging data were collected from 77 healthy controls (age: 37.8 ± 11.81 years). High-resolution T1-weighted anatomical scans, acquired using a multi-echo MPRAGE sequence, were used to construct the structural connectivity matrices. Resting-state functional MRI data, acquired using single-shot echo-planar imaging (EPI) aligned along the anterior commissure-posterior commissure (AC-PC) line, was used to estimate functional connectivity matrices. These matrices were averaged across subjects to produce a group-level functional connectivity matrix, which was subsequently used in downstream gradient analyses. The full set of parameters used in both imaging procedures can be found at

(COBRE documentation).

Connectome construction

T1-weighted images were processed using FreeSurfer (Fischl, 2012) and registered to the Lausanne500 atlas (Cammoun et al., 2013) to enable regional parcellation across both hemispheres (left: 225 regions, right: 223 regions). Both preprocessing and connectome construction were performed using the Connectome Reconstruction Toolbox (CATO) (de Lange et al., 2023), with default configurations. DWI images were preprocessed using FSL eddy, correcting for eddy current distortions within the data. Diffusion tensor imaging (DTI) was used to estimate the direction of white matter fibers within each voxel. Based on these estimates, deterministic fiber tracking, done within CATO, enabled reconstruction of the structural connectome. Structural connectivity (SC) within each hemisphere was quantified using volume-corrected streamline values-defined as the number of streamlines between two regions divided by their average volume

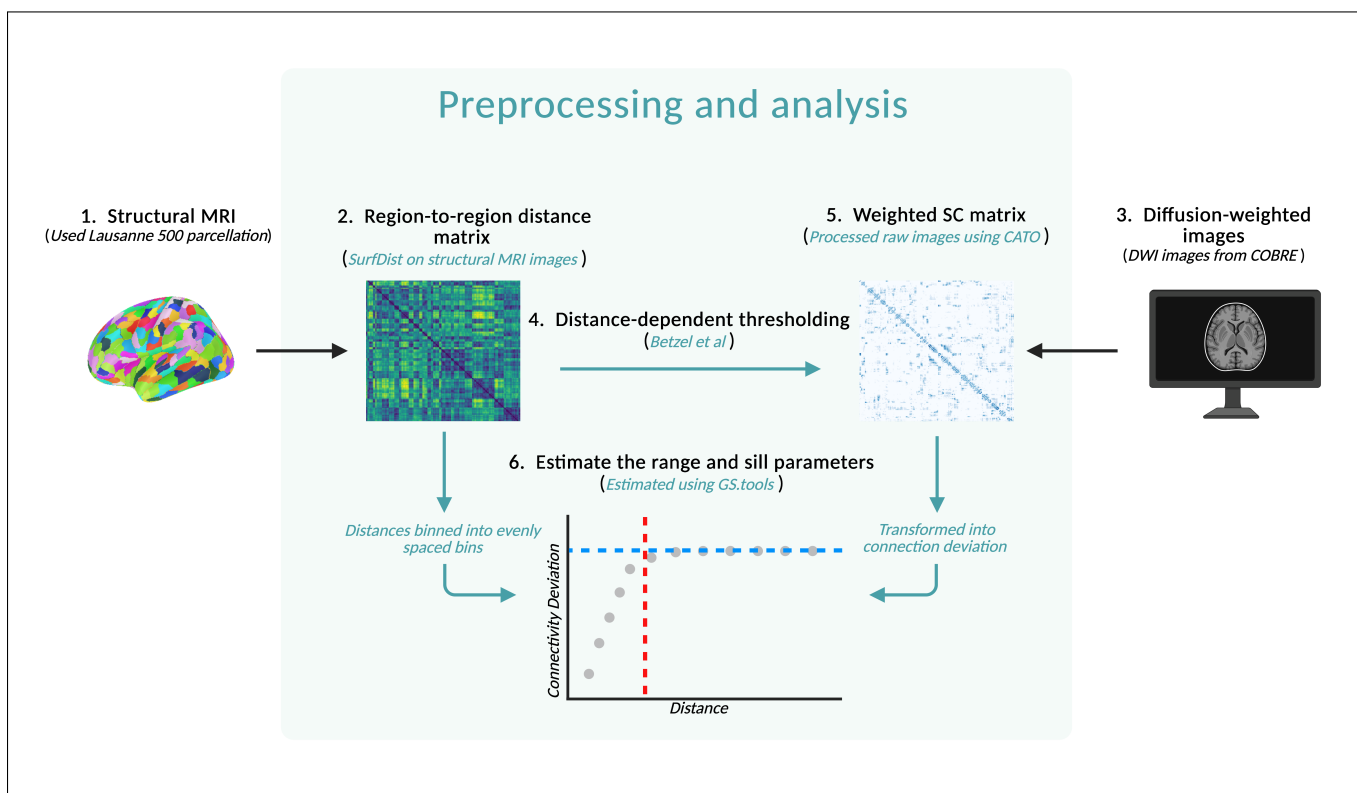


Figure 3: Overview of the methodological pipeline. White and blue indicate input data and intermediate processing steps, respectively. (1) Structural T1-weighted MRI scans from the COBRE dataset ($n = 77$) were parcellated using the Lausanne 500 atlas. (2) Region-to-region geodesic distances were computed along the cortical surface using SurfDist (Margulies et al., 2016a), then normalised by each subject's intracranial volume (ICV) and rescaled using the group-mean ICV. (3) Diffusion-weighted images were processed using CATO, resulting in weighted structural connectivity (SC) matrices. (4) Geodesic distance matrices were then used to apply distance-dependent thresholding to the SC matrices, preserving long-range structural connections (Betzel et al., 2019). Thresholded SC matrices were averaged across subjects to produce a group-level matrix. (5) The thresholded SC matrices were transformed into deviation profiles, enabling structural connectivity to be modeled as a function of distance. (6) Variograms were fitted to each region's deviation profile to estimate two parameters: the **range** (blue), indicating how far structural connectivity extends, and the **sill** (red), representing the strongest connection strength. Figure created with BioRender.

(Luppi et al., 2024; Heuvel and Sporns, 2011). Throughout this study, we refer to these values as connection strengths. To ensure a more balanced representation of both short- and long-range connections in the group-level structural connectivity (SC) matrix, distance-dependent thresholding was applied (Betzel et al., 2019). This approach more closely preserves the connection-length distribution, helping to retain long-range connections and potentially allowing for improved differentiation between unimodal and transmodal areas (Betzel et al., 2019). Each subject's SC matrix was first converted into a binary matrix indicating presence or absence of connections. Next, we divided connections into 41 equally spaced distance bins and computed the proportion of total streamlines in each bin (Kritikaki et al., 2024; Betzel et al., 2019). This proportion was scaled by the average streamline count across subjects to determine how many expected connections (EC) to retain per bin. Connections in each bin were ranked by prevalence across subjects, and only the top EC connections were retained. The resulting binary distance-dependent matrices, (left hemisphere: 4,613 connections, right hemisphere: 4,615 connections), were then weighted by the group averaged volume-corrected connection weights, producing the final weighted, undirected SC matrices used for subsequent analyses.

Geodesic distance

Geodesic distance (GD) between cortical regions was computed by estimating the centroid of each region. Regional centroids were defined by averaging the coordinates of all vertices within a region to approximate the center of mass, then selecting the vertex closest to this point (based on Euclidean distance) as the centroid (Yang et al., 2021). Pairwise centroid-to-centroid GDs were then calculated using SurfDist (Margulies et al., 2016a). To generate a group-level GD matrix, each subject's GD matrix was first normalised by their individual intracranial volume (ICV). These normalised matrices were then rescaled by the mean ICV across all subjects and averaged to produce group-level GD matrices for each hemisphere.

Model and parameter selection

Using existing Python-based tools, we applied a variogram-based framework (Müller et al., 2022) to model how connectivity changes with distance. To align with

this framework, we transformed each region's connectivity profile into a deviation metric by subtracting the strength of each connection from the region's strongest connection (see **Figure 2**). This captures the tendency for regions to exhibit their strongest connections locally (Markov et al., 2011), with connectivity declining over distance (Shinn et al., 2022; Leech et al., 2023). To stabilise model fitting and reduce noise, connectivity values were first binned into 20 equally spaced distance intervals. Several functions were then tested to see which best described how connectivity changes with distance. Although exponential functions are commonly used to model spatial connectivity (Shinn et al., 2022; Leech et al., 2023), we found that a Gaussian function better captured the global deviation pattern. This likely reflects the effect of binning and data sparsity, which may cause early saturation and deviation from exponential decay (see Supplementary).

Regional variograms

To estimate region-specific connectivity profiles, region-wise model fitting was applied. Following the same binning procedure used in the global model (Leech et al., 2023), volume-normalised connections were smoothed using a Gaussian kernel ($\sigma = 7$; see Supplementary). For each region, a Gaussian function was fitted to capture how much its connectivity deviates with increasing distance from its strongest connection. From this curve, two key parameters were extracted. The first is the sill, which reflects the maximum observed deviation in connectivity, that is, the drop in strength from the strongest to the weakest connections. Because the minimum connection strength approaches zero at large geodesic distances, the sill effectively corresponds to the region's strongest connection and thus serves as a proxy for peak local connectivity. The second is the range, defined as the distance at which 95% of this deviation is reached, providing an estimate of how far a region's connections typically extend across the brain (see **Figure 2**). These parameters were computed for all regions and used in subsequent analyses, with model fits consistently high across hemispheres ($R^2 = 0.98 \pm 0.0079$ left; $R^2 = 0.98 \pm 0.0099$ right).

Gradient construction

To define the unimodal-transmodal gradient, functional rather than structural connectivity was used. This was

done as structural connectivity gradients tend to follow an anterior-posterior axis, which makes it difficult to distinguish between sensory and transmodal areas (Wang et al., 2023), whereas functional connectivity gradients more clearly separate sensory-motor from transmodal cortices (Margulies et al., 2016b). The principal gradient was derived using nonlinear dimensionality reduction (Laplacian eigenmaps) applied to the group-average matrix, computed separately for each hemisphere using the BrainSpace toolbox (Vos de Wael et al., 2020).

Significance testing

To assess whether spatial connectivity features (range and sill) were significantly associated with cortical hierarchy, we calculated Spearman rank correlations between each region's position along the principal functional connectivity gradient and its corresponding range or sill values. These correlations served as the observed values. To generate null distributions, we randomly shuffled the range or sill values across regions 100,000 times, recalculating the correlation each time while keeping gradient values fixed. Two-tailed p-values were computed as the proportion of permuted correlations greater than or equal to the observed values. Additionally, to evaluate whether primary sensory regions showed a stronger relationship between connectivity features and cortical distance, we calculated Spearman correlations between each feature (range and sill) and the mean geodesic distance from four sensory anchor regions: V1 (pericalcarine), S1 (postcentral), M1 (precentral), and A1 (transverse temporal gyrus). These served as the observed values. We then repeated the analysis 100,000 times, each time selecting four random non-primary regions as anchors (excluding both the primary and selected regions), and recalculated the correlations. Null distributions were constructed from these values, and two-tailed p-values were calculated as the proportion of permuted correlations greater than or equal to the observed values.

Results

Quantifying Spatial Connectivity Patterns

To assess whether general connectivity trends align with previous findings (Betzel et al., 2016; Leech et al., 2023; Shinn et al., 2022), we first examined the relationship

between structural connectivity and distance across the cortex. As expected, the strongest connections were local: the top 5% of connection strengths occurred at an average distance of 22.5mm (left hemisphere) and 22.8mm (right hemisphere), compared to a average distance of 82.1mm (left) and 82.9mm (right) across all nonzero connections. Next, to explore whether broader patterns of cortical organisation are reflected in regional connectivity profiles, we estimated two parameters for each region: the range, indicating how far a region's connections typically extend, and the sill, representing its strongest connection and serving as a proxy for local connectivity strength (see **Figure 2**) (Buckner and Krienen, 2013; Sepulcre et al., 2010; Oligschläger et al., 2017, 2019). While not absolute measures, these parameters provide useful heuristics for comparing spatial patterns across the cortex.

Spatial range and sill patterns differentiate transmodal cortex

We found that, on average, transmodal regions exhibited longer spatial ranges and lower sill values following variogram analysis (see **Figure 4b**). This pattern suggests that these regions are less connected to adjacent areas but maintain connections that extend farther across the brain. The extended range aligns with prior functional imaging and structural connectivity studies (Oligschläger et al., 2019, 2017), which show that association cortices support long-distance communication. Furthermore, the observation that regions with shorter connection ranges exhibit stronger local connectivity, while those with longer ranges show weaker local coupling, may reflect a trade-off between the lower metabolic costs associated with short-range connectivity and the higher energetic demands of sustaining long-range communication (Bullmore and Sporns, 2012; Buzsáki et al., 2004).

In contrast, primary sensorimotor (unimodal) regions exhibited more strongly localised connectivity, characterised by shorter connection distances and higher local connection strengths (see **Figure 4b**). This pattern was consistent across both hemispheres, with connectivity ranges for these regions averaging 6mm shorter than those of transmodal regions in the right hemisphere ($p = 1.8 \times 10^{-8}$) and 7mm shorter in the left hemisphere ($p = 2.5 \times 10^{-12}$). Sill values, reflecting the strength of a region's strongest local connection, were also higher in unimodal areas, av-

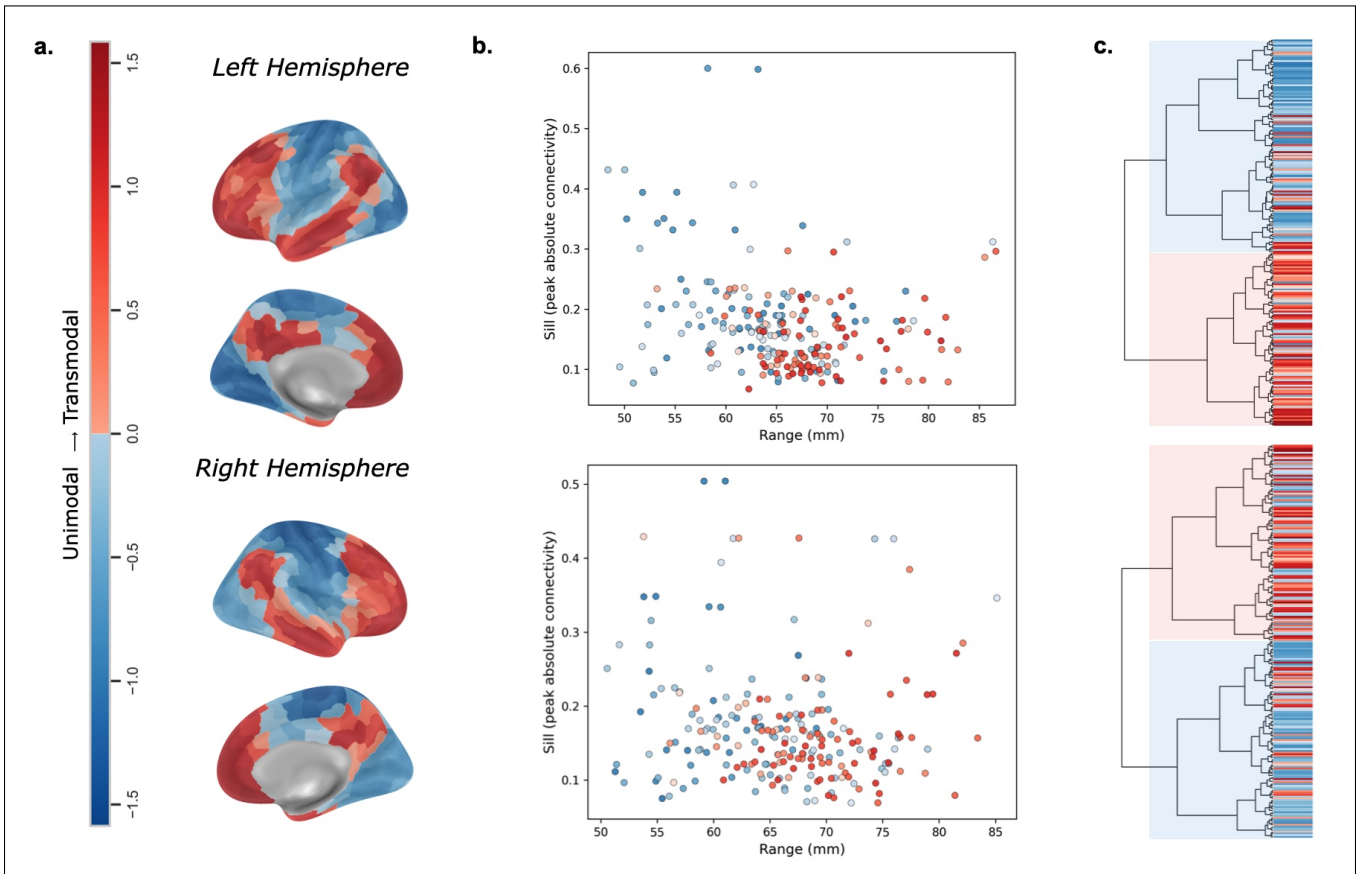


Figure 4: Spatial connectivity features and their organisation along the unimodal–transmodal axis. Each cortical region was characterised by two spatial connectivity features: *range*, indicating the typical length of its connections, and *sill*, reflecting the strength of its strongest local connection. Regions are coloured by their position along the principal functional connectivity gradient, with red indicating transmodal association cortex and blue indicating unimodal areas. (a) Z-scored principal functional gradient values projected onto the cortical surface, capturing each region’s position along the unimodal–transmodal axis (see *Gradient construction* for details). (b) Scatterplot showing how regions (dots) differ in connection length and strength (*range* and *sill*), coloured by gradient value (left hemisphere: 225 regions; right hemisphere: 223 regions). (c) Agglomerative hierarchical clustering (Ward’s method) applied to *range* and *sill* grouped regions into two major clusters. These broadly correspond to the unimodal–transmodal axis: the blue cluster includes regions with stronger local connectivity and shorter ranges (unimodal), while the red cluster includes regions with weaker local connectivity and longer-range projections (transmodal).

eraging 0.019 higher than transmodal regions in the right hemisphere ($p = 0.074$), and 0.049 higher in the left hemisphere ($p = 8.6 \times 10^{-6}$). To further test whether spatial connectivity estimates reflect cortical organisation, we computed Spearman correlations between each region’s functional gradient value and its connectivity features. Here, an association means that regions with higher values on the gradient (i.e., more transmodal) tend to show different connectivity features than regions with lower values (i.e., more unimodal). In the left hemisphere, range was positively associated with cortical hierarchy ($r = 0.26$, $p_{\text{perm}} = 0.00014$), while sill showed no significant association ($r = -0.09$, $p_{\text{perm}} = 0.1905$). A similar trend was observed in the right hemisphere (range: $r = 0.18$, $p_{\text{perm}} = 0.00723$; sill: $r = -0.12$, $p_{\text{perm}} = 0.0844$), suggesting that connection length more closely follows the unimodal–transmodal axis than connectivity strength, possibly because the sill is based on a single shared connec-

tion and therefore is more prone to noise.

Clustering of cortical hierarchies

Having shown that both a region’s strongest connection (sill) and its connection length (range) reflect key features of cortical organisation, we tested whether these measures could be used to cluster the cortex along the unimodal–transmodal axis. Using agglomerative hierarchical clustering (see Supplementary), we identified two principal clusters that broadly aligned with this hierarchy (blue: unimodal; red: transmodal) (see **Figure 4c**). Regions with stronger local connections and shorter connection lengths clustered as unimodal cortex, while those with weaker local connectivity and longer connection lengths formed a transmodal cluster. These results suggest that the spatial properties of structural connectivity capture biologically meaningful dimensions of large-scale cortical organisation.

Range and sill reflect proximity to primary areas

Motivated by the tethering hypothesis (Mesulam, 1990; Buckner and Krienen, 2013; Oligschläger et al., 2017, 2019), we tested whether connectivity range and sill values vary with distance from primary sensory regions (pericalcarine (V1), postcentral (S1), precentral (M1), and transverse temporal gyrus (A1)). We computed Spearman correlations between each non-primary region's mean geodesic distance from these anchors and its corresponding range and sill values.

Strong positive correlations were observed for range in both hemispheres (left: $r = 0.41, p = 4.1 \times 10^{-9}, p_{\text{perm}} = 0.012$; right: $r = 0.44, p = 1.36 \times 10^{-10}, p_{\text{perm}} = 0.0095$), indicating that regions farther from primary areas tend to support longer-range connectivity. Conversely, sill values showed modest negative correlations with distance (left: $r = -0.34, p = 1.46 \times 10^{-6}, p_{\text{perm}} = 0.065$; right: $r = -0.26, p = 2.12 \times 10^{-4}, p_{\text{perm}} = 0.099$), indicating a weak, non-significant association between proximity to primary areas and stronger local connectivity. To

better visualise how distance from primary sensory regions relates to the connectivity estimates, we projected both range and sill values onto the cortical surface (see **Figure 5a,c**). We also considered whether the observed connectivity features are influenced by a region's spatial position within the cortex. To examine this, we computed the mean distance from each region to all others and correlated these values with the estimated connectivity features (range and sill). We found that both connection range and local connectivity strength were associated with a region's average position across the cortex. Specifically, regions with greater mean distance to others tended to exhibit longer connection lengths (left: $r = 0.410, p = 1.51 \times 10^{-10}$; right: $r = 0.368, p = 1.52 \times 10^{-8}$) and, to a lesser extent, weaker local connectivity (left: $r = -0.33, p = 1.91 \times 10^{-6}$; right: $r = -0.310, p = 2.31 \times 10^{-6}$). This likely reflects the spatial necessity for longer connections in regions that are more peripherally located within the cortex (Oligschläger et al., 2019) and, coupled with findings that distance from primary sensorimotor areas influences connectivity, sug-

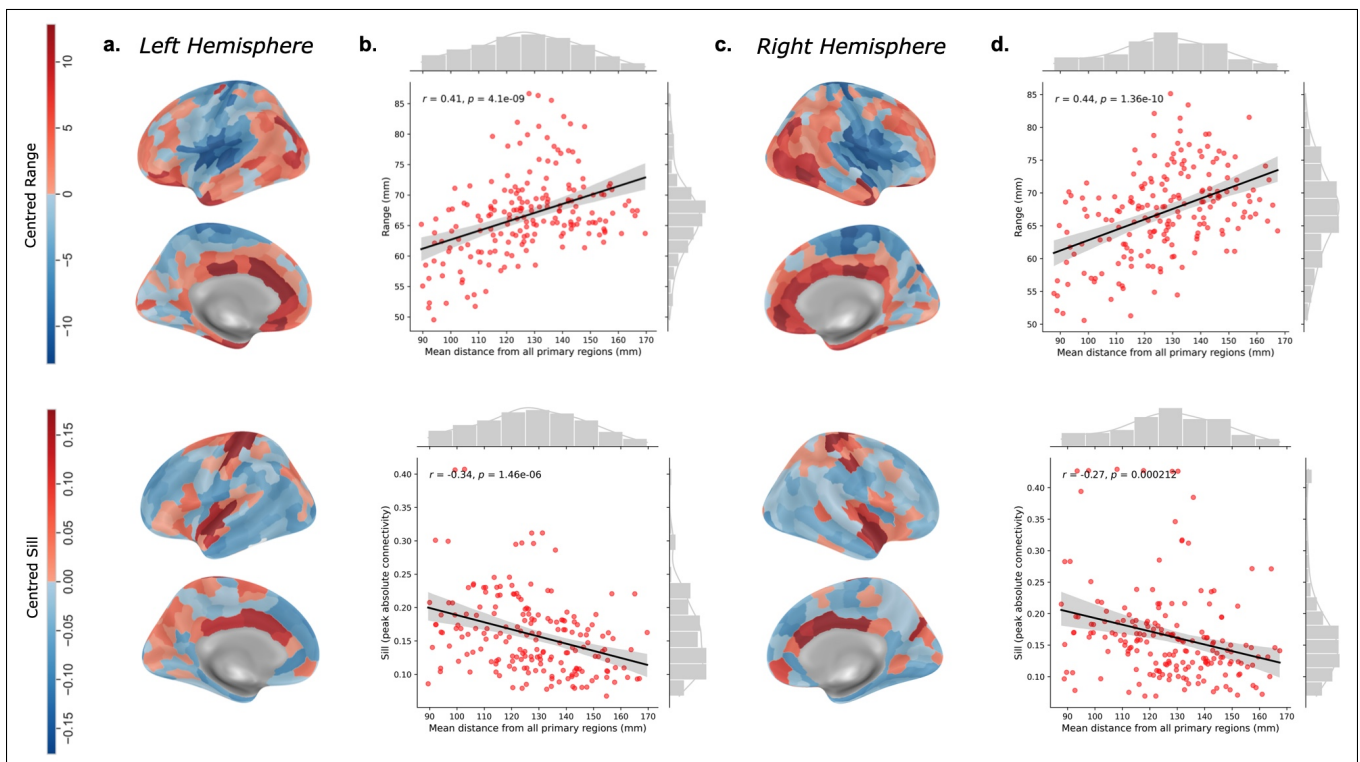


Figure 5: Cortical connectivity patterns and their relationship to distance from primary sensory regions. Two features were estimated for each cortical region: *range*, which captures how far a region typically connects across the cortex (i.e., connection length), and *sill*, which reflects the strength of a region's strongest local connection. These values were projected onto the cortical surface, with red indicating above-average values and blue indicating below-average values. (a) Left hemisphere surface maps: the top panel shows connection range, with longer-range connections found in transmodal areas; the bottom panel shows sill, with stronger local connections observed in primary sensorimotor regions. (b) Scatter plots for the left hemisphere: the top plot shows the relationship between connection range and distance from primary sensory anchors (V1, S1, M1, A1); the bottom plot shows the relationship between sill and anchor distance. (c) Right hemisphere surface maps: the top panel shows connection range; the bottom panel shows sill, revealing similar spatial distributions as in the left hemisphere. (d) Scatter plots for the right hemisphere, with the same layout as (b), showing consistent trends in both connection range (top) and local connectivity strength (bottom) relative to anchor distance.

a.	Hemisphere	Regions	Range	Sill	Hemisphere	Regions	Range	Sill	c.
LEFT (Low range, Low sill)	LEFT (Low range, Low sill)	postcentral_14	50.88	0.07	RIGHT (Low range, Low sill)	paracentral_2	55.44	0.07	
		postcentral_13	52.93	0.09		supramarginal_7	52.06	0.09	
		insula_3	49.53	0.10		insula_3	56.06	0.07	
		precentral_16	52.87	0.09		paracentral_4	54.88	0.09	
		superiorfrontal_5	62.27	0.06		postcentral_3	57.30	0.08	
	LEFT (Low range, High sill)	transversetemporal_1	48.37	0.43		superiortemporal_8	53.78	0.42	
		transversetemporal_2	50.03	0.43		precentral_16	53.80	0.34	
		precentral_1	50.22	0.34		insula_4	51.64	0.28	
		postcentral_1	51.79	0.39		precentral_15	54.87	0.34	
		insula_2	51.51	0.30		superiortemporal_5	50.56	0.25	
b.	LEFT (High range, Low sill)	temporalpole_1	81.94	0.07	RIGHT (High range, Low sill)	middletemporal_9	81.40	0.08	d.
entorhinal_1		78.04	0.08	entorhinal_1		74.57	0.06		
middletemporal_7		79.43	0.08	rostralanteriorcingulate_1		74.70	0.08		
rostralanteriorcingulate_1		75.56	0.08	parahippocampal_3		72.20	0.06		
superiorfrontal_6		71.34	0.08	medialorbitofrontal_5		74.37	0.09		
LEFT (High range, High sill)	caudalanteriorcingulate_2	86.64	0.31	posteriorcingulate_3		85.12	0.34		
	posteriorcingulate_2	86.34	0.29	caudalanteriorcingulate_1		77.38	0.38		
	caudalanteriorcingulate_1	85.55	0.28	superiortemporal_7		82.11	0.28		
	posteriorcingulate_1	82.88	0.31	caudalanteriorcingulate_3		75.97	0.42		
	precentral_5	77.74	0.22	medialorbitofrontal_2		81.53	0.27		

Table 1: Combinations of fitted sill and range parameters, alongside the top five cortical regions observed for each profile. A combined rank score was computed by ranking regions in ascending order based on their sill and range values, then summing the ranks to summarise each region's profile. Here, _n denotes a specific subregion belonging to the parent region (i.e., precentral_1 belongs to the precentral region). (a) Combinations of low range/low sill and low range/high sill in the left hemisphere, primarily mapped to primary sensory and unimodal regions exhibiting strong, spatially constrained local connectivity. (b) High range/low sill and high range/high sill combinations in the left hemisphere, typically observed in transmodal association areas with more spatially distributed but weaker local connectivity. (c) The same low-range parameter combinations in the right hemisphere, reflecting a similar pattern of spatial organisation. (d) High-range profiles in the right hemisphere, again mapping to transmodal regions, including areas implicated in the default mode network.

gests that both absolute and relative cortical positioning shape network organisation.

Discussion

Large-scale cortical organisation influences how each region connects with the rest of the brain, with primary sensory areas typically supporting dense local connections and transmodal regions exhibiting more distributed connectivity profiles (Sepulcre et al., 2010; Oligschläger et al., 2019). In this study, we characterised this organisation using two features: the strength of a region's strongest local connection (sill) and the typical length of its connections (range). We observed a spatial gradient in which unimodal regions tended to have shorter connection lengths and stronger local coupling, while transmodal regions more often showed longer-range connections and weaker local connectivity (Sepulcre et al., 2010). Connection length was significantly associated with cortical hierarchy, whereas local connection strength showed weaker alignment, suggesting that typical connection length may more

reliably reflect large-scale structural organisation. Together, these findings support the idea that distance from primary sensory regions helps shape the distribution of long-range connections across the cortex, consistent with the 'tethering hypothesis' (Buckner and Krienen, 2013).

Strong local connectivity was typically concentrated in primary motorsensory regions, particularly those involved in auditory and somatomotor processing. This was most evident in the transverse temporal, precentral, and postcentral gyri, as well as in certain regions of the superior temporal gyrus (see Table 1), in line with previous work showing that early sensory areas are dominated by short-range interactions (Wang et al., 2022; Sepulcre et al., 2010). A notable exception to this pattern was the pericalcarine (primary visual, V1) cortex. While it showed moderately strong local connectivity, it also exhibited extended connection lengths. This likely reflects projections along the ventral visual stream to inferior temporal areas (Hebart and Hesselmann, 2012; Bull and Zhang, 2021), but may also result from its posterior position in the brain,

requiring longer connections to reach anterior regions (Oligschläger et al., 2019). It should be noted that while V1 shows extended connectivity ranges, it is generally characterised by strong, short-range connectivity within the visual cortex (Sepulcre et al., 2010; Oligschläger et al., 2019).

Transmodal regions exhibited significantly longer connectivity ranges compared to unimodal areas, with the greatest ranges observed in regions linked to the default mode network (DMN), a system that has undergone substantial expansion during primate evolution (Hill et al., 2010; Wei et al., 2019). These included the middle temporal gyrus, rostral anterior cingulate, and superior frontal cortex (Sepulcre et al., 2010) (see **Table 1b, d** and Supplementary). Interestingly, these areas have been shown to lie at maximal distances from primary sensory regions (Oligschläger et al., 2019), suggesting that their spatial separation may contribute to a more distributed connectivity profile. Supporting this, we found a positive relationship between connection length and distance from primary anchors (see **Figure 5**), whereby greater mean distances from all primary regions was associated with increased connectivity ranges. Furthermore, while transmodal regions generally showed weaker local connectivity compared to unimodal areas, some regions displayed a hybrid profile, combining strong local and long-range connections. This pattern was particularly evident within regions of the cingulate cortex, namely the posterior and caudal anterior regions, recognised as core hubs of the default mode network (DMN) (Leech and Sharp, 2014; Gowik et al., 2023) (see **Table 1b, d; Figure 5**; and Supplementary). Consistent with this, these regions have also been identified as long-distance hubs in functional connectivity studies (Achard et al., 2006; Buckner et al., 2009; Sepulcre et al., 2010), reinforcing their role as integrative nodes within networks of the brain. This combination of local strength and extended projections reflects their function in linking nearby and distant processes within the DMN (Leech and Sharp, 2014; Gowik et al., 2023).

Connectivity profiles across the cortex revealed two broad organisational patterns: regions with strong local connectivity and short-range connections, typically seen in unimodal areas, and regions with weaker local connectivity and longer connection lengths, characteristic of transmodal cortex (Sepulcre et al., 2010). This contrast may

reflect a trade-off between the lower wiring costs of short-range connections and the integrative advantages of long-range connectivity (Jones and Powell, 1970; Mesulam, 1990, 1998; Buzsáki et al., 2004). The pattern aligns with small-world principles (Bassett and Bullmore, 2006; Ma et al., 2021), where dense local connections support specialised processing, while a smaller number of long-range connections link distant regions to enable efficient global communication at minimal cost (Bullmore and Sporns, 2012; Collin et al., 2014; Hahn et al., 2015). In addition to these connectivity patterns, a region's position within the cortex also influenced its connectivity profile. Regions located farther from others (i.e., more peripheral regions) tended to have longer connections and weaker local connectivity. This likely reflects the necessity for connections in peripheral regions to span greater distances in order to maintain communication, as well as broader organisational principles shaping network structure (Oligschläger et al., 2019). According to the tethering hypothesis (Buckner and Krienen, 2013), greater distance from early-developing sensory and motor areas may allow for increased functional differentiation. Together, these findings suggest that both a region's location in the cortical sheet and its proximity to primary regions shape the development of more distributed, integrative connectivity patterns, especially in higher-order association areas.

Limitations

This study has several limitations. Structural connectivity reconstructed from diffusion tensor imaging (DTI) is known to include a high number of false-positive connections (Rostampour et al., 2023), which may lead to overestimated connection ranges. Future studies could address this by using group-level thresholding methods that better balance false positives and false negatives (de Reus and van den Heuvel, 2013). Increasing sample sizes and incorporating non-human primate data would also help determine whether the observed patterns generalize across individuals and species. Additionally, due to the sparsity of structural connectivity matrices, applying a Gaussian smoothing filter introduces a trade-off between reducing noise and preserving meaningful signal. Although we attempted to mitigate this by selecting a sigma value that yielded stable R^2 and RMSE estimates (see Supplementary), some degree of trend distortion due to smoothing

remains possible. Finally, because the sill is based on a single strongest connection per region, it may be particularly sensitive to noise or false positives, making it a less robust estimate of local connectivity strength. Future work could explore alternative summary measures, such as averaging the top percentile of strongest connections, to provide more stable estimates of local coupling.

Conclusion

Regional connectivity profiles were examined across the human brain to assess whether features such as local connection strength and connection length reflect broader organisational principles. We found that a region's typical connection length reiterated its position along the unimodal-transmodal axis, where unimodal regions were characterised by short-range connectivity, while transmodal regions exhibited longer-range connections. These differences in range estimates showed stronger alignment with the cortical hierarchy, whereas local connectivity strength demonstrated weaker association. This suggests that connection range, rather than local connectivity strength, more effectively captures the large-scale transition from sensory to higher-order processing. Supporting the 'tethering hypothesis' (Buckner and Krienen, 2013), we observed that regions farther from primary sensory areas tended to have longer connection lengths, consistent with the idea that proximity to early-developing sensory regions may constrain network development. Additionally, regions situated more peripherally within the cortex showed both longer connection distances and weaker local connectivity, suggesting that spatial position itself contributes to shaping regional connectivity profiles. Together, these findings indicate that both cortical location and distance from primary anchors influence the organisation of connectivity ranges.

Supporting information

Additional figures and methodological details, including parameter choices, are provided in the attached Supplementary PDF. All code used in this study is available at: github.com/gabrielhaw/ConnectomeEvo

Acknowledgments

I would like to thank Prof. Martijn van den Heuvel for his guidance throughout the internship, and Bernardo Maciel

and Sebastian Quiroz Monnens for their help and input at various stages of the project.

References

- S. Achard, R. Salvador, B. Whitcher, J. Suckling, and E. Bullmore. A resilient, low-frequency, small-world human brain functional network with highly connected association cortical hubs. *Journal of Neuroscience*, 26(1):63–72, 2006. doi: 10.1523/JNEUROSCI.3874-05.2006.
- D. S. Bassett and E. Bullmore. Small-world brain networks. *The Neuroscientist*, 12(6):512–523, 2006. doi: 10.1177/1073858406293182.
- R. F. Betzel, A. Avena-Koenigsberger, J. Goñi, Y. He, M. A. de Reus, A. Griffa, P. E. Vértes, B. Mišić, J.-P. Thiran, P. Hagmann, M. van den Heuvel, X.-N. Zuo, E. T. Bullmore, and O. Sporns. Generative models of the human connectome. *NeuroImage*, 124:1054–1064, Jan. 2016. ISSN 1053-8119. doi: 10.1016/j.neuroimage.2015.09.041. URL <https://www.sciencedirect.com/science/article/pii/S1053811915008563>.
- R. F. Betzel, A. Griffa, P. Hagmann, and B. Mišić. Distance-dependent consensus thresholds for generating group-representative structural brain networks. *Network Neuroscience*, 3(2):475–496, Mar. 2019. ISSN 2472-1751. doi: 10.1162/netn_a_00075. URL <https://www.ncbi.nlm.nih.gov/pmc/articles/PMC6444521/>.
- R. L. Buckner and F. M. Krienen. The evolution of distributed association networks in the human brain. *Trends in Cognitive Sciences*, 17(12):648–665, Dec. 2013. ISSN 1364-6613, 1879-307X. doi: 10.1016/j.tics.2013.09.017. URL [https://www.cell.com/trends/cognitive-sciences/abstract/S1364-6613\(13\)00221-0](https://www.cell.com/trends/cognitive-sciences/abstract/S1364-6613(13)00221-0). Publisher: Elsevier.
- R. L. Buckner, J. Sepulcre, T. Talukdar, F. M. Krienen, H. Liu, T. Hedden, J. R. Andrews-Hanna, R. A. Sperling, and K. A. Johnson. Cortical hubs revealed by intrinsic functional connectivity: mapping, assessment of stability, and relation to alzheimer's disease. *Journal of Neuroscience*, 29(6):1860–1873, 2009. doi: 10.1523/JNEUROSCI.5062-08.2009.
- D. R. Bull and F. Zhang. Chapter 2 - The human visual system. In D. R. Bull and F. Zhang, editors, *Intelligent Image and Video Compression (Second Edition)*, pages 17–58. Academic Press, Oxford, Jan. 2021. ISBN 978-0-12-820353-8. doi: 10.1016/B978-0-12-820353-8.00011-6. URL <https://www.sciencedirect.com/science/article/pii/B9780128203538000116>.
- E. Bullmore and O. Sporns. The economy of brain network organization. *Nature Reviews Neuroscience*, 13(5):336–349, Apr. 2012. ISSN 1471-0048. doi: 10.1038/nrn3214.
- G. Buzsáki, C. Geisler, D. A. Henze, and X.-J. Wang. Interneuron Diversity series: Circuit complexity and axon wiring economy of cortical interneurons. *Trends in Neurosciences*, 27(4):186–193, Apr. 2004. ISSN 0166-2236, 1878-108X. doi: 10.1016/j.tins.2004.02.007. URL [https://www.cell.com/trends/neurosciences/abstract/S0166-2236\(04\)00064-5](https://www.cell.com/trends/neurosciences/abstract/S0166-2236(04)00064-5). Publisher: Elsevier.
- L. Cammoun, X. Gigandet, D. Meskaldji, J.-P. Thiran, O. Sporns, K. Q. Do, P. Maeder, R. Meuli, and P. Hagmann. Mapping the human connectome at multiple scales with diffusion spectrum mri. *NeuroImage*, 68:117–129, 2013. doi:

- 10.1016/j.neuroimage.2012.11.048. URL <https://www.sciencedirect.com/science/article/pii/S0165027011005991>.
- R. Chin, S. W. C. Chang, and A. J. Holmes. Beyond cortex: The evolution of the human brain. *Psychological Review*, 130(2): 285–307, 2023. ISSN 1939-1471. doi: 10.1037/rev0000361. Place: US Publisher: American Psychological Association.
- G. Collin, O. Sporns, R. C. W. Mandl, and M. P. van den Heuvel. Structural and functional aspects relating to cost and benefit of rich club organization in the human cerebral cortex. *Cerebral Cortex (New York, N.Y.: 1991)*, 24(9):2258–2267, Sept. 2014. ISSN 1460-2199. doi: 10.1093/cercor/bht064.
- S. C. de Lange, K. Helwegen, and M. P. van den Heuvel. Structural and functional connectivity reconstruction with cato—a connectivity analysis toolbox. *NeuroImage*, 273:120108, 2023. doi: 10.1016/j.neuroimage.2023.120108. URL <https://pubmed.ncbi.nlm.nih.gov/37059156/>.
- M. A. de Reus and M. P. van den Heuvel. Estimating false positives and negatives in brain networks. *NeuroImage*, 70: 402–409, 2013. ISSN 1053-8119. doi: 10.1016/j.neuroimage.2012.12.066.
- B. Fischl. Freesurfer. *NeuroImage*, 62(2):774–781, 2012. doi: 10.1016/j.neuroimage.2012.01.021. URL <https://www.ncbi.nlm.nih.gov/pmc/articles/PMC3685476/>. Author manuscript; available in PMC: 2013 Jun 18.
- J. K. Gowik, C. Goelz, S. Vieluf, F. van den Bongard, and C. Reinsberger. Source connectivity patterns in the default mode network differ between elderly golf-novices and non-golfers. *Scientific Reports*, 13(1):6215, Apr. 2023. ISSN 2045-2322. doi: 10.1038/s41598-023-31893-1. URL <https://www.nature.com/articles/s41598-023-31893-1>. Publisher: Nature Publishing Group.
- A. Hahn, G. S. Kranz, R. Sladky, S. Ganger, C. Windischberger, S. Kasper, and R. Lanzenberger. Individual diversity of functional brain network economy. *Brain Connectivity*, 5(3): 156–165, Apr. 2015. ISSN 2158-0022. doi: 10.1089/brain.2014.0306.
- M. N. Hebart and G. Hessmann. What Visual Information Is Processed in the Human Dorsal Stream? *Journal of Neuroscience*, 32(24):8107–8109, June 2012. ISSN 0270-6474, 1529-2401. doi: 10.1523/JNEUROSCI.1462-12.2012. URL <https://www.jneurosci.org/content/32/24/8107>. Publisher: Society for Neuroscience Section: Journal Club.
- M. P. v. d. Heuvel and O. Sporns. Rich-Club Organization of the Human Connectome. *Journal of Neuroscience*, 31(44):15775–15786, Nov. 2011. ISSN 0270-6474, 1529-2401. doi: 10.1523/JNEUROSCI.3539-11.2011. URL <https://www.jneurosci.org/content/31/44/15775>. Publisher: Society for Neuroscience Section: Articles.
- J. Hill, T. Inder, J. Neil, D. Dierker, J. Harwell, and D. Van Essen. Similar patterns of cortical expansion during human development and evolution. *Proceedings of the National Academy of Sciences*, 107(29):13135–13140, July 2010. doi: 10.1073/pnas.1001229107. URL <https://www.pnas.org/doi/full/10.1073/pnas.1001229107>. Publisher: Proceedings of the National Academy of Sciences.
- E. G. Jones and T. P. Powell. An anatomical study of converging sensory pathways within the cerebral cortex of the monkey. *Brain*, 93(4):793–820, 1970. doi: 10.1093/brain/93.4.793.
- E. Kritikaki, M. Mancini, D. Kyriazis, N. Sigala, S. F. Farmer, and L. Berthonze. Constructing representative group networks from tractography: lessons from a dynamical approach. *Frontiers in Network Physiology*, 4, Nov. 2024. ISSN 2674-0109. doi: 10.3389/fnetp.2024.1457486. URL <https://www.frontiersin.org/journals/network-physiology/articles/10.3389/fnetp.2024.1457486/full>. Publisher: Frontiers.
- R. Leech and D. J. Sharp. The role of the posterior cingulate cortex in cognition and disease. *Brain*, 137(1):12–32, Jan. 2014. ISSN 0006-8950. doi: 10.1093/brain/awt162. URL <https://www.ncbi.nlm.nih.gov/pmc/articles/PMC3891440/>.
- R. Leech, R. Vos De Wael, F. Váša, T. Xu, R. Austin Benn, R. Scholz, R. M. Braga, M. P. Milham, J. Royer, B. C. Bernhardt, E. J. H. Jones, E. Jefferies, D. S. Margulies, and J. Smallwood. Variation in spatial dependencies across the cortical mantle discriminates the functional behaviour of primary and association cortex. *Nature Communications*, 14: 5656, Sept. 2023. ISSN 2041-1723. doi: 10.1038/s41467-023-41334-2. URL <https://www.ncbi.nlm.nih.gov/pmc/articles/PMC10499916/>.
- A. I. Luppi, S. P. Singleton, J. Y. Hansen, K. W. Jamison, D. Bzdok, A. Kuceyeski, R. F. Betzel, and B. Misic. Contributions of network structure, chemoarchitecture and diagnostic categories to transitions between cognitive topographies. *Nature Biomedical Engineering*, 8(9):1142–1161, Sept. 2024. ISSN 2157-846X. doi: 10.1038/s41551-024-01242-2. URL <https://www.nature.com/articles/s41551-024-01242-2>. Publisher: Nature Publishing Group.
- J. Ma, J. Zhang, Y. Lin, and Z. Dai. Cost-efficiency trade-offs of the human brain network revealed by a multiobjective evolutionary algorithm. *NeuroImage*, 236:118040, 2021. doi: 10.1016/j.neuroimage.2021.118040. URL <https://www.sciencedirect.com/science/article/pii/S1053811921003177>.
- D. S. Margulies, M. Falkiewicz, and J. M. Huntenburg. A cortical surface-based geodesic distance package for Python. *GigaScience*, 5(suppl_1):s13742-016-0147-0-q, Nov. 2016a. ISSN 2047-217X. doi: 10.1186/s13742-016-0147-0-q. URL <https://doi.org/10.1186/s13742-016-0147-0-q>.
- D. S. Margulies, S. S. Ghosh, A. Goulas, M. Falkiewicz, J. M. Huntenburg, G. Langs, G. Bezgin, S. B. Eickhoff, F. X. Castellanos, M. Petrides, E. Jefferies, and J. Smallwood. Situating the default-mode network along a principal gradient of macroscale cortical organization. *Proceedings of the National Academy of Sciences*, 113(44):12574–12579, Nov. 2016b. doi: 10.1073/pnas.1608282113. URL <https://www.pnas.org/doi/full/10.1073/pnas.1608282113>. Publisher: Proceedings of the National Academy of Sciences.
- N. T. Markov, P. Misery, A. Falchier, C. Lamy, J. Vezoli, R. Quilodran, M. A. Gariel, P. Giroud, M. Ercsey-Ravasz, L. J. Pilaz, C. Huissoud, P. Barone, C. Dehay, Z. Toroczkai, D. C. Van Essen, H. Kennedy, and K. Knoblauch. Weight Consistency Specifies Regularities of Macaque Cortical Networks. *Cerebral Cortex*, 21(6):1254–1272, June 2011. ISSN 1047-3211. doi: 10.1093/cercor/bhq201. URL <https://doi.org/10.1093/cercor/bhq201>.
- M. M. Mesulam. Large-scale neurocognitive networks and distributed processing for attention, language, and memory. *Annals of Neurology*, 28(5):597–613, Nov. 1990. ISSN 0364-5134. doi: 10.1002/ana.410280502.

- M. M. Mesulam. From sensation to cognition. *Brain: A Journal of Neurology*, 121 (Pt 6):1013–1052, June 1998. ISSN 0006-8950. doi: 10.1093/brain/121.6.1013.
- S. Müller, L. Schüler, A. Zech, and F. Heße. GSTools v1.3: a toolbox for geostatistical modelling in Python. *Geoscientific Model Development*, 15(8):3161–3176, 2022. doi: 10.5194/gmd-15-3161-2022. URL <https://gmd.copernicus.org/articles/15/3161/2022/>. © Author(s) 2022. This work is distributed under the Creative Commons Attribution 4.0 License.
- S. Oligschläger, J. M. Huntenburg, J. Golchert, M. E. Lauckner, T. Bonnen, and D. S. Margulies. Gradients of connectivity distance are anchored in primary cortex. *Brain Structure and Function*, 222(5):2173–2182, July 2017. ISSN 1863-2661. doi: 10.1007/s00429-016-1333-7. URL <https://doi.org/10.1007/s00429-016-1333-7>.
- S. Oligschläger, T. Xu, B. M. Baczkowski, M. Falkiewicz, A. Falchier, G. Linn, and D. S. Margulies. Gradients of connectivity distance in the cerebral cortex of the macaque monkey. *Brain Structure and Function*, 224(2):925–935, Mar. 2019. ISSN 1863-2661. doi: 10.1007/s00429-018-1811-1. URL <https://doi.org/10.1007/s00429-018-1811-1>.
- OpenAI. Chatgpt (june 2024 version). <https://chat.openai.com>, 2024. Large language model developed by OpenAI.
- T. M. Preuss. The human brain: rewired and running hot. *Annals of the New York Academy of Sciences*, 1225(Suppl 1):E182–E191, May 2011. ISSN 0077-8923. doi: 10.1111/j.1749-6632.2011.06001.x. URL <https://www.ncbi.nlm.nih.gov/pmc/articles/PMC3103088/>.
- M. G. Rosa and R. Tweedale. Brain maps, great and small: lessons from comparative studies of primate visual cortical organization. *Philosophical Transactions of the Royal Society B: Biological Sciences*, 360(1456):665–691, Apr. 2005. doi: 10.1098/rstb.2005.1626. URL <https://royalsocietypublishing.org/doi/10.1098/rstb.2005.1626>. Publisher: Royal Society.
- M. Rostampour, Z. Gharaylou, A. Rostampour, F. Shahbodaghy, M. Zarei, R. Fadaei, and H. Khazaie. Study of structural network connectivity using DTI tractography in insomnia disorder. *Psychiatry Research: Neuroimaging*, 336:111730, Dec. 2023. ISSN 0925-4927. doi: 10.1016/j.psychresns.2023.111730. URL <https://www.sciencedirect.com/science/article/pii/S0925492723001403>.
- J. Sepulcre, H. Liu, T. Talukdar, I. Martincorena, B. T. T. Yeo, and R. L. Buckner. The Organization of Local and Distant Functional Connectivity in the Human Brain. *PLOS Computational Biology*, 6(6):e1000808, June 2010. ISSN 1553-7358. doi: 10.1371/journal.pcbi.1000808. URL <https://journals.plos.org/ploscompbiol/article?id=10.1371/journal.pcbi.1000808>. Publisher: Public Library of Science.
- M. Shinn, A. Hu, L. Turner, S. Noble, K. H. Preller, J. L. Ji, F. Moujaes, S. Achard, D. Scheinost, R. T. Constable, J. H. Krystal, F. X. Vollenweider, D. Lee, A. Anticevic, E. T. Bullmore, and J. D. Murray. Spatial and temporal autocorrelation weave complexity in brain networks, Apr. 2022. URL <https://www.biorxiv.org/content/10.1101/2021.06.01.446561v2>. Pages: 2021.06.01.446561 Section: New Results.
- M. V. Suntsova and A. A. Buzdin. Differences between human and chimpanzee genomes and their implications in gene expression, protein functions and biochemical properties of the two species. *BMC Genomics*, 21(7):535, Sept. 2020. ISSN 1471-2164. doi: 10.1186/s12864-020-06962-8. URL <https://doi.org/10.1186/s12864-020-06962-8>.
- R. Vos de Wael, O. Benkarim, C. Paquola, S. Larivière, J. Royer, S. Tavakol, T. Xu, S.-J. Hong, G. Langs, S. Valk, B. Misić, M. Milham, D. Margulies, J. Smallwood, and B. C. Bernhardt. BrainSpace: a toolbox for the analysis of macroscale gradients in neuroimaging and connectomics datasets. *Communications Biology*, 3(1):1–10, Mar. 2020. ISSN 2399-3642. doi: 10.1038/s42003-020-0794-7. URL <https://www.nature.com/articles/s42003-020-0794-7>. Publisher: Nature Publishing Group.
- Y. Wang, J. Royer, B.-y. Park, R. Vos de Wael, S. Larivière, S. Tavakol, R. Rodriguez-Cruces, C. Paquola, S.-J. Hong, D. S. Margulies, J. Smallwood, S. L. Valk, A. C. Evans, and B. C. Bernhardt. Long-range functional connections mirror and link microarchitectural and cognitive hierarchies in the human brain. *Cerebral Cortex (New York, NY)*, 33(5):1782–1798, May 2022. ISSN 1047-3211. doi: 10.1093/cercor/bha0172. URL <https://www.ncbi.nlm.nih.gov/pmc/articles/PMC9977370/>.
- Y. Wang, J. Royer, B.-y. Park, R. Vos de Wael, S. Larivière, S. Tavakol, R. Rodriguez-Cruces, C. Paquola, S.-J. Hong, D. S. Margulies, J. Smallwood, S. L. Valk, A. C. Evans, and B. C. Bernhardt. Long-range functional connections mirror and link microarchitectural and cognitive hierarchies in the human brain. *Cerebral Cortex*, 33(5):1782–1798, Mar. 2023. ISSN 1047-3211. doi: 10.1093/cercor/bhac172. URL <https://doi.org/10.1093/cercor/bhac172>.
- Y. Wei, S. C. de Lange, L. H. Scholtens, K. Watanabe, D. J. Ardesch, P. R. Jansen, J. E. Savage, L. Li, T. M. Preuss, J. K. Rilling, D. Postuma, and M. P. van den Heuvel. Genetic mapping and evolutionary analysis of human-expanded cognitive networks. *Nature Communications*, 10:4839, 2019. doi: 10.1038/s41467-019-12764-8. URL <https://www.nature.com/articles/s41467-019-12764-8>.
- S. Yang, K. Wagstyl, Y. Meng, X. Zhao, J. Li, P. Zhong, B. Li, Y.-S. Fan, H. Chen, and W. Liao. Cortical patterning of morphometric similarity gradient reveals diverged hierarchical organization in sensory-motor cortices. *Cell Reports*, 36(8), Aug. 2021. ISSN 2211-1247. doi: 10.1016/j.celrep.2021.109582. URL [https://www.cell.com/cell-reports/abstract/S2211-1247\(21\)01016-0](https://www.cell.com/cell-reports/abstract/S2211-1247(21)01016-0). Publisher: Elsevier.